TITANIUM OXIDE NANOTUBES DECORATED WITH RUTHENIUM OXIDE NANOPARTICLES FOR PHOTODEGRADATION OF MALACHITE GREEN, METHYLENE BLUE, AND INDIGO CARMINE

by

Jonathan Daniel Buford

APPROVED BY SUPERVISORY COMITTTEE:

Kenneth J. Balkus, Jr., Chair

John P. Ferraris

Paul Pantano

I dedicate this to my family and friends who have loved and supported me

TITANIUM OXIDE NANOTUBES DECORATED WITH RUTHENIUM OXIDE NANOPARTICLES FOR PHOTODEGRADATION OF MALACHITE GREEN, METHYLENE BLUE, AND INDIGO CARMINE

by

Jonathan Daniel Buford, BS

THESIS

Presented to the Faculty of

The University of Texas at Dallas

in Partial Fulfillment

of the Requirements

for the Degree of

MASTER OF SCIENCE IN

CHEMISTRY

THE UNIVERSITY OF TEXAS AT DALLAS

December 2018

ACKNOWLEDGEMENTS

I would like to thank my research supervisor, Dr. Kenneth J. Balkus Jr., for his guidance throughout my graduate student career. The knowledge that he has imparted to me, as well as the learning environment, has allowed me to understand chemistry. The knowledge that I was able to obtain in his lab not only helped to further my comprehension of chemistry, but my understanding of how it applies to the real world. I am grateful for the advice he has given me and to have been a part of his lab during my time at UTD. I would also like to express my appreciation for Dr. John P. Ferraris for also advancing my knowledge by providing another perspective for my research and results. While here, he has also helped immensely by allowing me to use his instruments and facilities to conduct my experiments. I would like to express thanks to Dr. Duck J. Yang and Dr. Paul Pantano for providing helpful suggestions during meetings that have guided me.

Another group of people I would like to thank are the members of the Balkus lab, who have during my time at UTD helped me via consulting for research projects, while also being supportive and making my time in the lab memorable. My appreciation also goes out to Betty Maldonado, Dr. George D. McDonald, and Dr. Winston Layne of the chemistry department staff. Lastly, I would like to thank my mother Sherry Buford, my father Richard Buford, and my brother Landon Buford for their love and support.

November 2018

TITANIUM OXIDE NANOTUBES DECORATED WITH RUTHENIUM OXIDE NANOPARTICLES FOR PHOTODEGRADATION OF MALACHITE GREEN, METHYLENE BLUE, AND INDIGO CARMINE

Jonathan Daniel Buford, MS

The University of Texas at Dallas, 2018

Supervising Professor: Kenneth J. Balkus, Jr.

Titanium dioxide (TiO_2) is the most widely studied material for photodegradation of organic contaminants thanks to its activity as well as the abundance, low-cost, and multiple nanostructures (particles, rods, and tubes). TiO_2 nanotubes are of interest because of their high surface area and have been modified with many metal-based nanoparticles to increase photocatalytic activity. In this thesis TiO_2 nanotubes decorated with 1-5nm diameter ruthenium oxide (RuO_2) nanoparticles were investigated. TiO_2 nanotubes decorated with green ruthenium oxide nanoparticles were successfully synthesized. The interaction between the RuO_2 nanoparticles and TiO_2 nanotubes (TNTs) shifted the XPS Ti $2p_{3/2}$ peak spectra to a lower binding energy, supporting that the nanoparticles were bound to the TNTs. The RuO_2-decorated TNTs were tested as photocatalysts for the photodegradation of three dyes: malachite green (cationic dye), methylene blue (cationic dye), and indigo carmine (anionic dye). The malachite green and methylene blue dyes adsorbed well to the surface of the RuO_2-decorated TNTs and

were degraded in 120 min and 240 min respectively. The indigo carmine dye did not display significant adsorption for the RuO_2-decorated TNTs, which had slower photodegradation than the bare TNTs, due to the anionic nature of the dye. The indigo carmine was only degraded to about 40% after 240 min. Overall the RuO_2 decorated TNTs performed best in cationic dyes where superior adsorption was displayed compared to the bare TNTs and previously reported RuO_2 decorated TiO_2 nanoparticles, but lower photodegradation rates were observed.

TABLE OF CONTENTS

LIST OF FIGURES

LIST OF TABLES

CHAPTER 1

INTRODUCTION

The amount of fresh water available on the planet is only about 2.5% of the total water amount, therefore the purification of contaminated water is an important area of research.[1] Organic dyes from textiles and water-treatments are common types of pollutants that are released into the environment as wastewater.[2-3] Many organic dyes are a threat to the health of plants, animals, and people.[2-3] A widely used method to treat various organic contaminants is photocatalysis.[4-6] Titanium dioxide has been the most studied material for photocatalysis since the splitting of water was detected on TiO_2 electrodes by Fujishima and Honda.[7] When TiO_2 is irradiated by UV-light, electrons and holes are produced which act as reductants and oxidants, respectively.[7-11] This results in the formation of reactive oxygen species such as the hydroxyl radical ($OH^{\bullet}$), singlet oxygen ($^1O_2$) and the superoxide anion ($O_2^{\bullet -}$), which breakdown organic contaminants.[9-10] TiO_2 is favored for photocatalysis due to its resistance to photocorrosion, abundance, low-toxicity, and low cost. The ability to separate electron-hole pairs depends on the nature of the band gap. TiO_2 has multiple crystalline phases. The most common crystalline phases are rutile and anatase. Rutile has a direct band gap of 3.0 eV while anatase has an indirect band gap of 3.2 eV which makes anatase the preferred crystalline phase.[11-14] Different TiO_2 morphologies including nanoparticles, nanorods, and nanotubes have been studied to increase the surface area and photocatalytic activity.[11, 15-16] Nanotubes have the highest surface area of the three morphologies (~345 m^2/g) allowing for more reactive surfaces to be

available.[11, 13, 17] Although TiO_2 has many benefits for photocatalysis it also has shortcomings. The large band gap makes it difficult to utilize sunlight energy.[8, 18-21]

In order to enhance the photocatalytic performance of TiO_2 the attachment of various types of nanoparticles have been studied.[18-19, 21-23] One of the more interesting nanoparticle materials that has been studied is ruthenium oxide.[24-25] Ruthenium oxide is known to be an efficient water oxidation catalyst.[26-27] Ruthenium oxide was recently shown to improve the performance of the TiO_2 by serving as a metal-like material heightening charge separation, which helps generate more radical species.[21] The improved charge separation occurs because of bending energy bands caused by electron transfer between TiO_2 and RuO_2 to balance the Fermi level.[21] RuO_2 has a low band gap of 2.2 eV, which absorbs in the visible light region.[28] Upon UV irradiation the RuO_2 would form additional reactive species because of the transfer of photogenerated holes from the TiO_2, as shown in Fig. 1.[21] These photogenerated holes are produced from electrons excited from the TiO_2 valence band (E_{vb}) to the conduction band (E_{cb}) near the fermi level. Uddin et al. reported TiO_2 nanoparticles decorated with RuO_2 to degrade methylene blue.[21] Bavykin et al also used RuO_2-decorated TNTs to degrade alcohols.[24] Our study will center on photocatalysis of dye based contaminants that have not been tested using TNTs-decorated with RuO_2 nanoparticles. Our expectations of improved catalytic activity and the overall scarcity of studies on TNTs paired with RuO_2 nanoparticles prompted our research of using TiO_2 nanotubes decorated with RuO_2 nanoparticles for photocatalysis of other dyes focusing on differences in size and charge, as it has not been researched yet with these types of materials.[24-25]

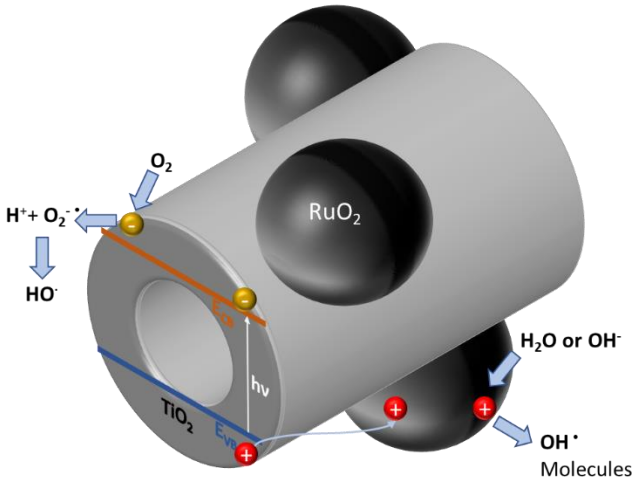

Figure 1. Diagram of UV-light irradiation induced charge separation at the TiO_2/RuO_2 interface of a RuO_2-decorated TNT and the reactive species generated.

The cationic dyes that were tested included malachite green and methylene blue (Table 1). Malachite green is used as a fungicide, an ectoparasiticide, and has a max absorption wavelength near 616 nm.[2, 29-30] Methylene blue, which is used as a textile dye, has a max absorption wavelength near 660 nm.[19, 31-37] In addition to the two cationic dyes of malachite green and methylene blue one anionic dye indigo carmine was tested. Indigo carmine is used as a food dye and has a max absorption wavelength at about 610 nm (Table 1).[38] All of the dyes will be in between pH 8 and pH 6 in order to mimic polluted waste streams.[39] The hydroxyl radicals are more common at neutral and high pH levels; while positively charged holes are more prevalent at low pH levels.[33, 40] Controlling the pH is also important because the pH of the dye solution affects the surface chemistry of the TiO_2. If the pH of the solution is above the

isoelectric point (pI) the surface of the TiO_2 will be negatively charged, while the surface will be positively charged if the solution's pH is below the pI.[19] As shown in equations (1) and (2):

(1) pH > pI: $Ti\text{-}OH + OH^- \leftrightarrow TiO^- + H_2O$

(2) pH < pI: $Ti\text{-}OH + H^+ \leftrightarrow TiOH_2^+$

Equation (1) and (2) refer to basic and acidic media respectively.[19] The pI of TiO_2 is typically around 6, but TiO_2 nanotubes have been shown to have negatively charged surfaces at the same pH and lower.[33, 36, 40] The pI for RuO_2 is 5.2, so the RuO_2 is expected to be negatively charged while in the dye solutions.[41] The charge state of TiO_2 and RuO_2 will be highly influential on the effectiveness of the RuO_2-decorated TNT catalyst in the cationic and anionic dyes.

CHAPTER 2

MATERIALS AND METHODS

2.1 Materials

All reagents were utilized as received without additional purification. Titanium oxide, Aeroxide® P25 was purchased from Acros Organics. The sodium hydroxide pellets were purchased from Macron. The 12M hydrochloric acid was purchased from Fisher Scientific. The cysteine (≥97%) was purchased from SAFC. The ruthenium (III) chloride hydrate was purchased from Pressure Chemical Company. The malachite green oxalate (>90%) was purchased from Avocado Research Chemicals. The methylene blue was purchased from Allied Chemical. The indigo carmine (98%) was purchased from Sigma-Aldrich.

2.2 TiO_2 Nanotube Synthesis

0.5 g of TiO_2/P25 was dispersed in 30 mL of DI water. Once a homogenous solution was obtained 10.5 g of NaOH were added to the solution. The solution was poured into a 40 ml Teflon liner and sealed in an autoclave for 24 h at 150 °C. The sample was then washed with DI water to a pH ~ 8.5 and then washed with 0.1 M HCl. The sample was dried at 85 °C in air and then annealed at 280 °C for 80 min.

2.3 Cysteine Treatment

3.2713 g of cysteine are dispersed in 30 mL of DI water to obtain a concentration of 0.9M. 0.25 grams of TiO_2 nanotubes are then added to the solution and stirred for 1 h in the dark. The

solution is centrifuged and washed with DI water three times to remove excess cysteine. The sample was then dried in air at 85°C. The same procedure was followed for the 0.6 M sample, 2.1809 g of cysteine are used.

2.4 Attachment of RuO_2 Nanoparticles

0.0188 g of $RuCl_3 \cdot nH_2O$ were dissolved in 20 mL of DI water and stirred at room temperature for 30 min. 0.125 g of cysteine-treated TiO_2 nanotubes were added to solution and stirred for 2 h. The solution was centrifuged and washed with DI water 3 times to remove unbound ruthenium. The ruthenium-treated TiO_2 nanotubes were mixed with 3 mL of a 1 M solution of NaOH and stirred for 2 h. The solution was centrifuged and washed again and dried in air at 85 °C. The sample was annealed at 250 °C for 80 min in air.

2.5 Dye Degradation

A 25 ppm solution was prepared by dissolving 0.025 g of each dye in 1 L of deionized water. For the photodegradation experiments 0.020 g of catalyst and 100 mL of dye solution were used for each trial. The reaction vessel was a 250-mL quartz round-bottom flask that was 20 cm from the light source. The experiment was done in a dark box with a water-cooled 450-W Hanovia quartz mercury UV-lamp. The solutions were irradiated for at most 240 min., with time zero being after the catalyst had been stirred in the dye solution for 1 h.

Table 1. Dye Solution Properties

Dye	λmax (nm)	Conc. (ppm) in water	Initial pH
Malachite Green 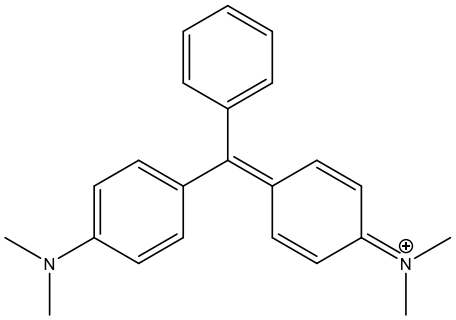	616	25	6.22
Methylene Blue 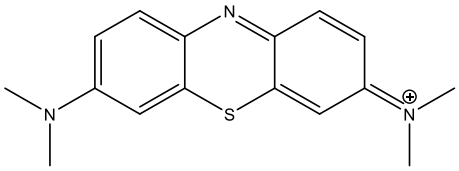	660	25	6.02
Indigo Carmine 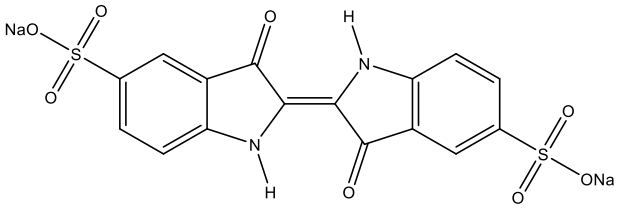	610	25	7.60

2.6 Characterizations

X-ray powder diffraction (XRD) was conducted on a Rigaku Ultima IV utilizing copper K-alpha radiation. The transmission electron microscopy (TEM) images were taken on a FEI CM200 FEG transmission electron microscope operating at 200 kV. Infrared spectra were obtained via Fourier transform infrared attenuated total reflection spectroscopy (FTIR-ATR) with a Nicolet380 FT-IR SmartOrbit ATR model spectrometer. X-ray photoelectron spectroscopy was conducted using a Perkin-Elmer PHI System equipped with an Al K-alpha X-ray source at a chamber base pressure of 1.5×10^{-9} Torr. The spectra were recorded with a 16-channel detector using a hemispherical analyzer. A Perkin-Elmer Lambda 900 UV-Vis-NIR spectrophotometer was used for the collection of the UV-vis-NIR reflectance spectra.

CHAPTER 3

RESULTS AND DISCUSSION

3.1 Characterization of TiO_2 nanotubes and RuO_2-decorated TiO_2 nanotubes

Fig. 2a shows TEM images of the as-synthesized TiO_2 nanotubes that are ~10 nm in diameter as well as, having a hollow-core with open ends. The TiO_2 nanotubes are multi-walled with pores of ~5 nm as shown by the TEM image in Fig.2b.

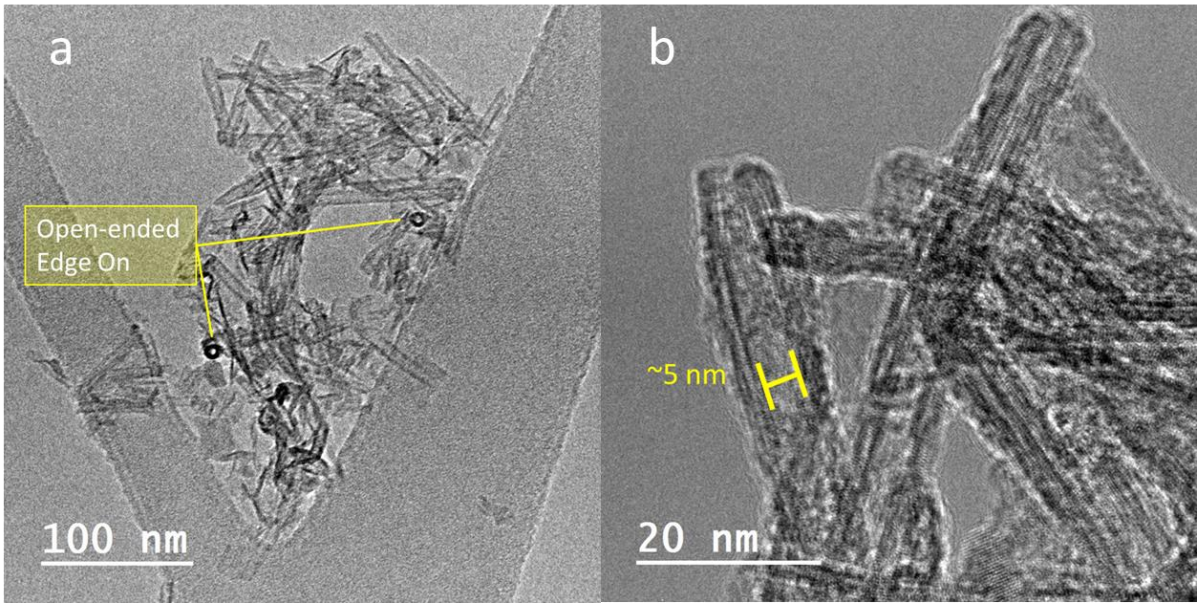

Figure 2. TEM images of the synthesized TiO_2 nanotubes at low and high magnification.

The lattice fringes in corresponding to the TiO_2 nanotubes TEM images show the ordered nature of the TiO_2 nanotubes confirmed by the X-ray diffraction in Fig.3 which shows the

nanotubes are anatase. The crystalline peaks match with the simulated pattern (JCPDS No:21-1272) indicating the anatase crystalline phase. N_2 adsorption results in a Brunauer–Emmett–Teller (BET) surface area of 285 m^2/g. TiO_2/P25 nanoparticles have a surface area of ~70 m^2/g.[21]

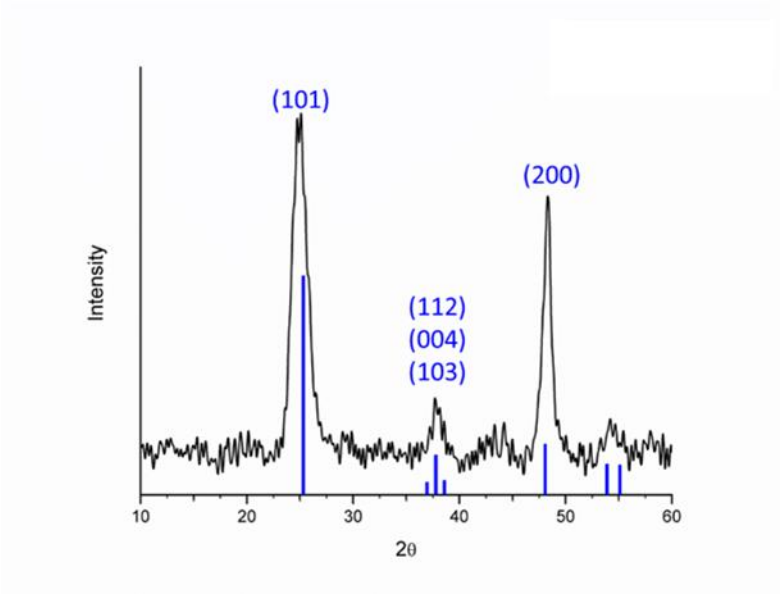

Figure 3. XRD pattern of TiO_2 nanotubes and the simulated pattern (JCPDS No:21-1272 pattern (blue)).

In order to control the size of the RuO_2 nanoparticles a cysteine linker is first bound to the TiO_2 nanotubes as shown in Fig.4. This method was implemented by Ratanatawanate et al. to control the sizes of PbS and CuS nanoparticles with more cysteine yielding bigger nanoparticles.[18-19]

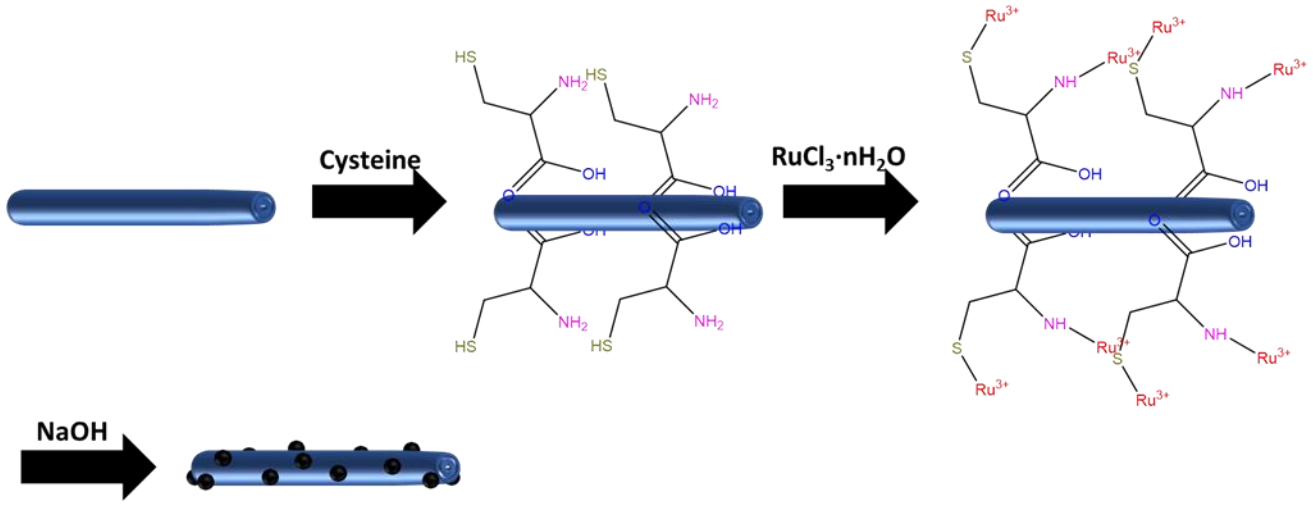

Figure 4. A schematic diagram of RuO_2 synthesis on a TiO_2 nanotube.

The spectrum in Fig. 5a shows is for bare TiO_2 nanotubes with a band near 3300cm^{-1} which is characteristic of hydroxyl groups from water. The spectrum in Fig. 5b shows bands near 3023 cm^{-1}, 2915 cm^{-1}, 2578 cm^{-1}, and 1619 cm^{-1} which represent amine, methylene, thiol, and carbonyl groups, respectively, that are characteristic of cysteine.[18] The spectrum in Fig. 5c is for TiO_2 nanotubes with bound 0.6 M cysteine which shows similar bands to the pure cysteine spectrum indicating the cysteine is bound, with the addition of a band near 3417 cm^{-1}. This band characteristic of a hydroxyl group and is being caused by water present on the TiO_2 nanotubes.[18] The red spectrum in Fig.5d is for 0.9 M RuO_2-decorated TNTs and shows a hydroxyl band near 3485 cm^{-1}, which is associated with water.

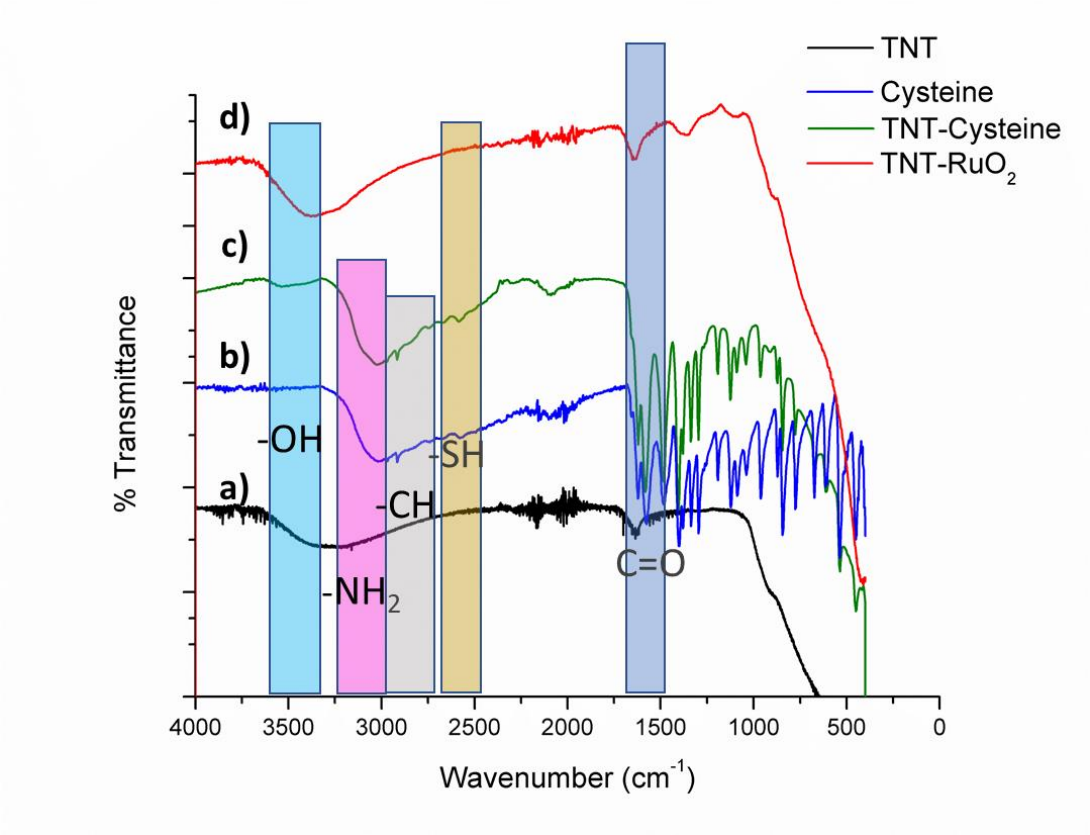

Figure 5. FTIR-ATR spectra of a) bare TiO_2 nanotubes (black), b) cysteine (blue), c) TiO_2 nanotubes with cysteine (green), and d) TiO_2 nanotubes with RuO_2 (red).

The RuO_2-decorated TNTs were characterized by TEM images shown in Fig.6. The nanoparticles were on the outside of the nanotube. In Fig. 6b the attached nanoparticles showed a d-spacing of about 0.168 nm. The 0.168 nm d-spacing corresponds to a 211 reflection. Fig. 6c shows the RuO_2 nanoparticles in the 0.6 M cysteine sample are in the size range of 1-2 nm for the bulk of the nanoparticles. Fig. 6d shows the size of the RuO_2 nanoparticles for the 0.9 M cysteine sample, which are between 3-4 nm for the bulk of the nanoparticles. The BET surface area for the 0.9 M cysteine RuO_2-decorated TNTs was measured to be 290 m^2/g. The presence of the

RuO_2 was shown with XRD in Fig.7. The TiO_2 shows the 101, 112, 104, 103, 200, 211, 105 reflections, while the RuO_2 was identified by the 110, 101, 211 reflections. The Scherrer equation calculated RuO_2 nanoparticles of ~2 nm and ~4 nm for the 0.6 M and 0.9 M, respectively.

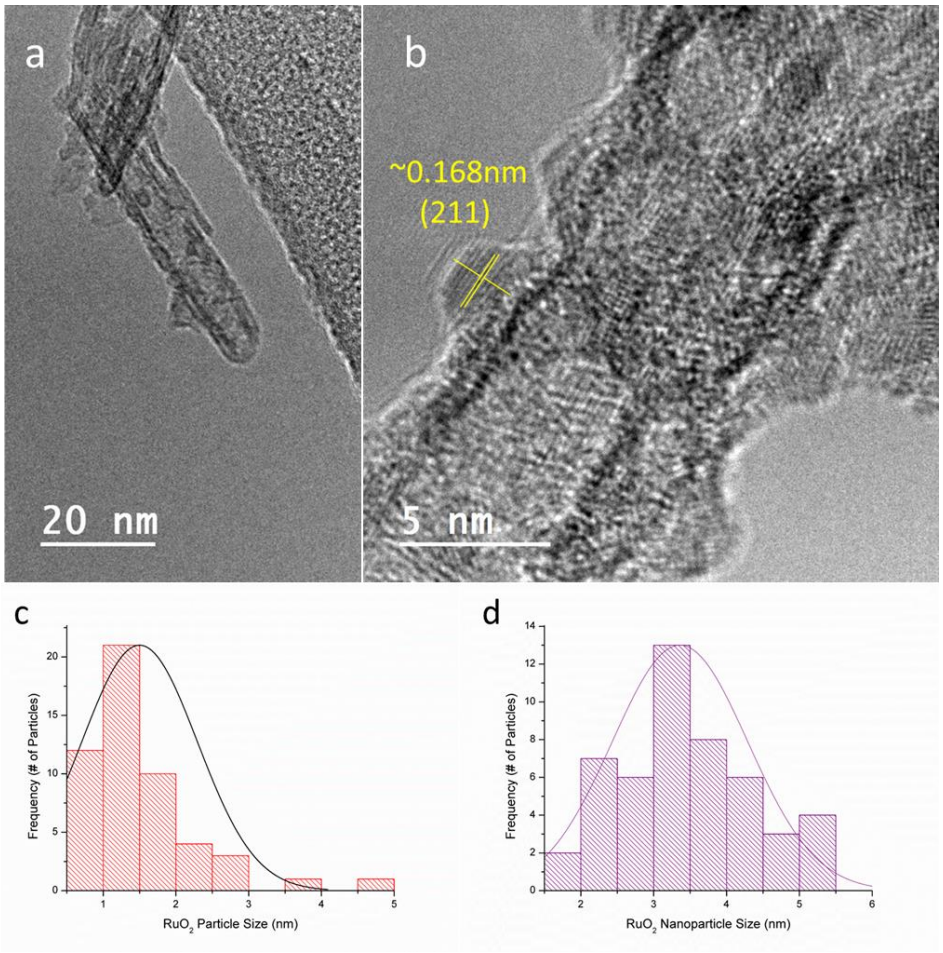

Figure 6. TEM images of a) and b) the synthesized RuO_2 decorated TiO_2 nanotubes at low and high magnification, c) a histogram of sizes for the 0.6 M cysteine RuO_2, and d) a histogram of sizes for the 0.9 M cysteine RuO_2.

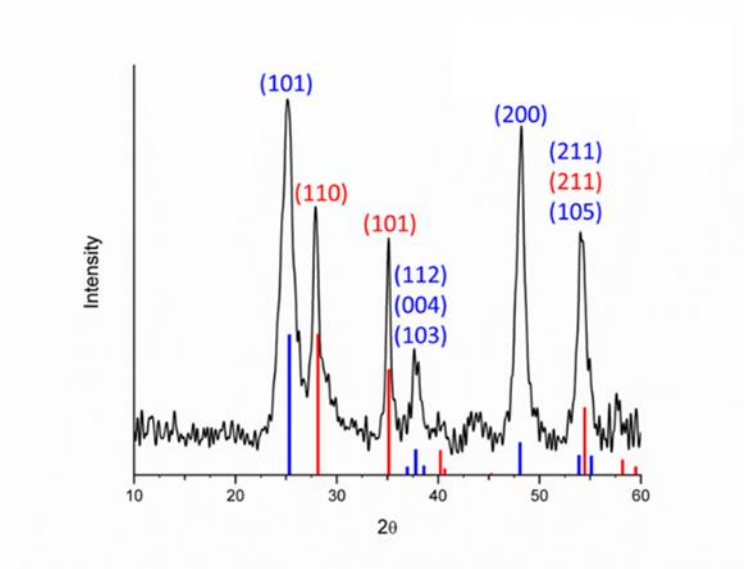

Figure 7. XRD pattern of 0.9 M RuO_2-decorated TNTs with anatase TiO_2 (JCPDS No:21-1272) and RuO_2 (JCPDS No:43-1027) simulated via blue and red patterns, respectively.

Uddin et al. used XPS to show that the RuO_2 nanoparticles were bound to TiO_2 nanoparticles due to a Ti $2p_{3/2}$ spectra shift to a lower binding energy that was attributed to band bending at the TiO_2/RuO_2 interface.[21] XPS was collected for the 0.6 M RuO_2-decorated TNTs and Figs. 8a and 8b show the survey XPS spectra of the bare TNTs and RuO_2 decorated TNTs.[42, 43] The inset in Fig. 8b shows a Ru $3d_{5/2}$ peak near 281 eV. In Fig. 8c two Ti 2p peaks are shown in the high-resolution XPS spectra for the bare TiO_2 nanotubes, Ti $2p_{1/2}$ and Ti $2p_{3/2}$ located at ~461 eV and 458.2 eV, respectively.[42] Fig.8d shows the deconvoluted Ti $2p_{1/2}$ and Ti $2p_{3/2}$ for the RuO_2-decorated TNTs. The deconvoluted spectra shows a new peak shifted to a lower binding energy. The shift from 458.2 eV to 457.4 eV is consistent with the directional shift observed by Uddin et al. that was associated with band bending (in this case the lowering of the conduction band) at

the RuO_2/TiO_2 heterojunction, meaning the RuO_2 nanoparticles are bound to the TiO_2 nanotubes (a potential Ru-O-Ti bond).[21] The heterojunction is a result of the TiO_2 and RuO_2 having different band gaps.[21] This may result in charge transfer between their conduction bands.[19, 21] Fig.8e and 8f represent the oxygen present in both the bare TNTs and the RuO_2 decorated TNTs. The TiO_2 and RuO_2 oxygen groups are both represented by the deconvoluted peak at the 530.4 eV binding energy and the adsorbed water is represented by the deconvoluted peak at the 531.6 eV binding energy for both Figs. 8e and 8f.[42-43] In Fig. 8f a third deconvoluted peak was at 534.8 eV which corresponds to a carbonyl group, this peak is either the result of contamination or it is residual carbon from the cysteine.[44]

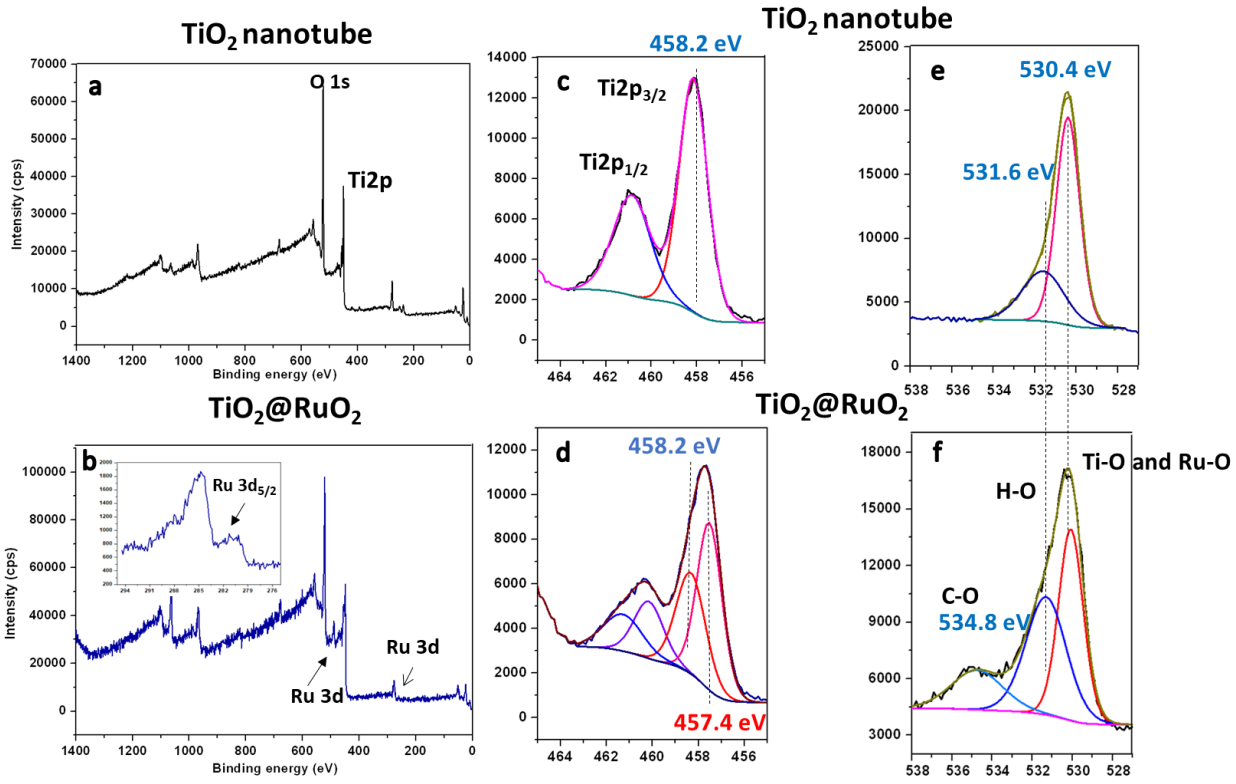

Figure 8. XPS spectra of a) the survey spectrum of TiO_2 nanotubes, b) the survey spectrum of RuO_2 decorated TiO_2 nanotubes, c) a high-resolution deconvoluted spectrum of the Ti 2p peaks (TNTs), d) a high-resolution deconvoluted spectrum of the Ti 2p peaks (RuO_2-decorated TNTs), e) a high-resolution deconvoluted spectrum of the oxygen peaks (TNTs), and f) a high-resolution deconvoluted spectrum of the oxygen peaks (RuO_2-decorated TNTs).

The RuO_2-decorated TiO_2 nanotubes displayed a green color. The solid-state UV-Vis spectra are displayed in Fig. 9. The RuO_2-decorated TiO_2 nanotubes have the mixed absorption properties of both TiO_2 nanotubes and RuO_2 particles (TiO_2/P25 was used as the blank). For both the RuO_2-decorated TNT samples (0.6 M and 0.9 M cysteine concentration) the maximum absorbance at ~300nm is maintained from the TiO_2 nanotubes. While also being comparable to the RuO_2 particles in absorption capability, except for an absorbance minimum near 600 nm in the visible

spectrum. A similar result was observed by Uddin et al. with an absorbance minimum occurring in the visible region for TiO_2 nanoparticles decorated with RuO_2.[21] Uddin et al. attributed the result to the excitement of multiple oscillating electrons (surface plasmon effect) at the interface of the RuO_2 nanoparticles and the TiO_2, which also decreased in the indirect band gap of the material by ~0.5 eV (in comparison to only the TiO_2).[21] In contrast, Ganguly et al. obtained similar results using only RuO_2 nanoparticles of ~7 nm size.[45] A similar result being obtained with only RuO_2 nanoparticles indicates that the result is simply related to the size of the RuO_2. The spectra were further analyzed using tauc plots in Fig. 10 to see if any band gap effects were observable. Fig. 10a the TiO_2 nanotubes (in blue) were calculated to have a band gap of 3.20 eV, which is expected for anatase. Fig.10b the RuO_2-decorated TNTs synthesized with 0.6 M cysteine (in light green) were calculated to have a band gap of 2.73 eV. Fig.10c the RuO_2-decorated TNTs synthesized with 0.9 M cysteine (in dark green) were calculated to have a band gap of 2.69 eV. These results indicate that the binding of the RuO_2 nanoparticles to the TiO_2 nanotubes does cause the band to bend. This band bending is indicated by the lowering of the band gap. These results also indicate that binding more RuO_2 lowers the band gap of the TiO_2 even further. Due to the 0.9 M sample having a lower band gap, the 0.6 M sample was not used for photodegradation experiments.

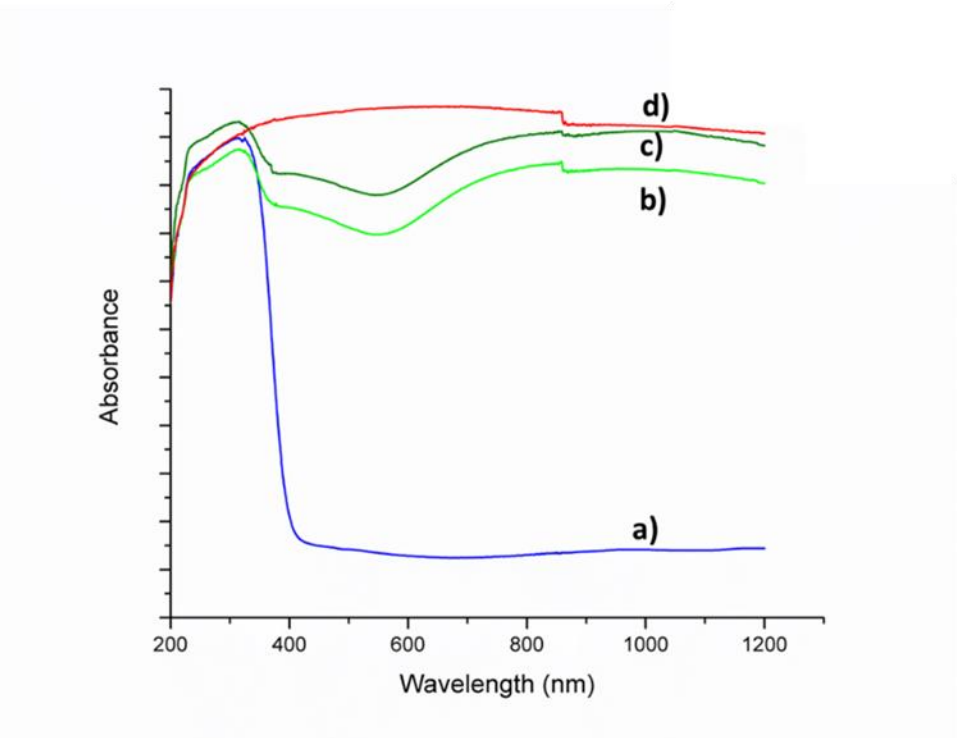

Figure 9. UV-Vis-NIR absorbance spectra for a) TiO_2 nanotubes (blue), TiO_2 nanotubes decorated with RuO_2 for b) 0.6 M (light green) and c) 0.9 M cysteine concentration (dark green), and d) RuO_2 particles (red).

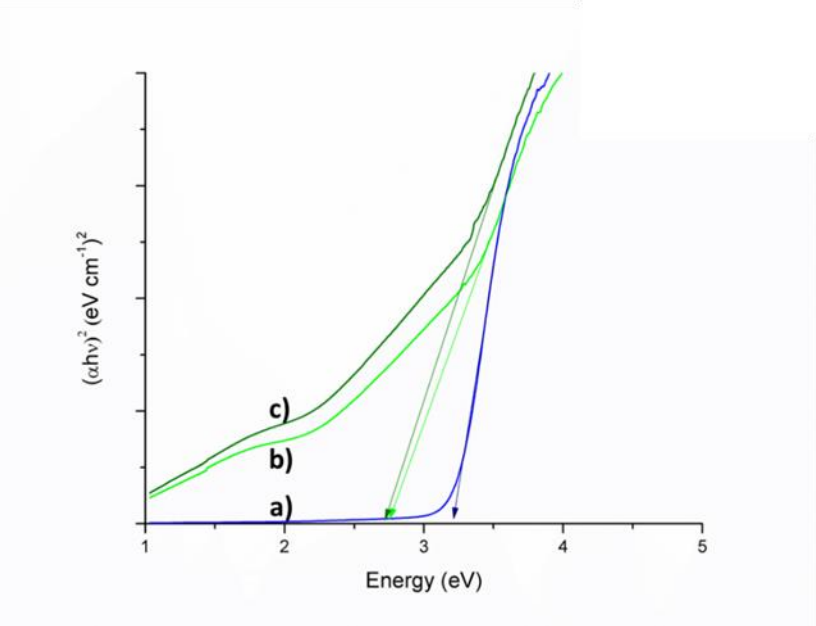

Figure 10. Tauc plot modeling the band gaps of a) TiO_2 nanotubes, b) TNTs-decorated with RuO_2 nanoparticles synthesized with 0.6 M cysteine concentration, and c) TNTs-decorated with RuO_2 nanoparticles synthesized with 0.9 M cysteine concentration.

3.2 Photocatalytic Activity

Figs. 11-13 show the results of the photodegradation and the 25 ppm degradation rates are shown in Table 2 of the malachite green, methylene blue, and indigo carmine dyes at room temperature. From Fig. 11, it is clear that after stirring in darkness for one hour the concentration of the malachite green dye is nearly 15% less for the RuO_2-decorated TNT catalyst. This difference in dye concentration is attributed to the adsorption quality of the RuO_2 decorated TNT catalyst. The bare TNT and RuO_2-decorated TNT catalyst degraded the malachite green dye by more than 95% after two hours. However, the applied reaction rate constant (k_{app}) for the RuO_2 decorated TNTs was 1.16×10^{-2} min^{-1} and 2.76×10^{-2} min^{-1} for the bare TNTs. The lower k_{app} for the RuO_2 decorated TNTs also makes the normalized reaction rate (K_{norm}),

calculated via the equation $K_{norm} = k_{app}/S_{BET}$ (S_{BET} = BET surface area), to be lower as well with K_{norm} being 3.99×10^{-5} g m^{-2} min^{-1} and 9.67×10^{-5} g m^{-2} min^{-1} for RuO_2 decorated TNTs and the bare TNTs, respectively. The pH of the stock solution of malachite green was measured to be 6.22 (adjusted with 1 M NaOH). After the reaction was finished the color of both catalysts changed, this was especially obvious in the case of the bare TiO_2 nanotubes which changed from white to black (RuO_2 decorated TNTs changed from green to black). These color changes indicate that malachite green related molecules are still on the surface of both catalysts.[19] These results indicate that for malachite green dye the RuO_2 decorated catalyst was only superior in terms of adsorption compared to the bare TNTs.

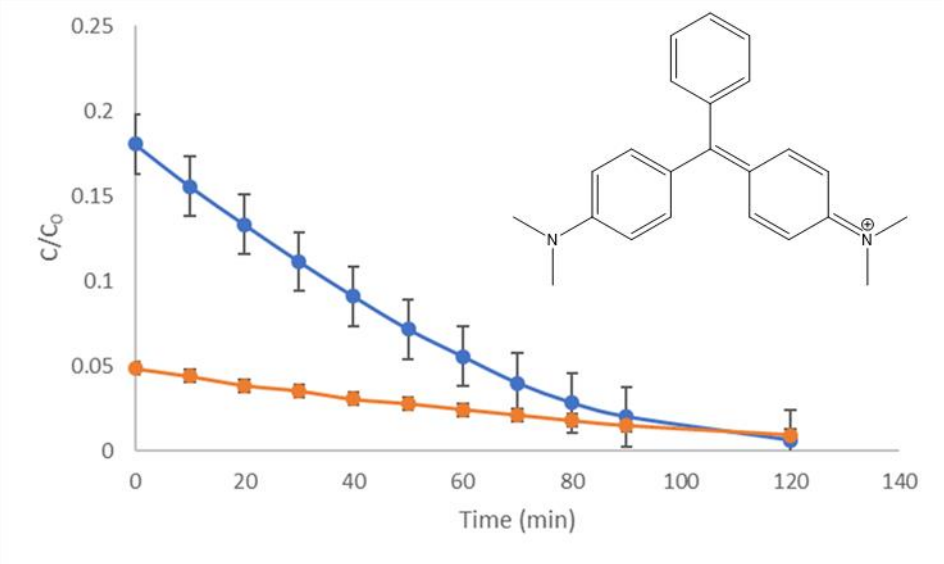

Figure 11. Plot displaying the dye concentration vs. irradiation time for the degradation of malachite green (inset) with TiO_2 nanotubes (—●—) and TiO_2 nanotubes decorated with RuO_2 (—■—).

The superiority of the RuO_2-decorated TNTs vs. the bare TNTs persist in 25 ppm methylene blue photodegradation (not shown) where the dye concentration is about 0.80 lower than the bare TNTs after stirring in darkness. The dye concentration percent is about the same as the malachite green dye than what was shown in Fig. 11, despite the smaller size of methylene blue molecules in comparison to the malachite green molecules. This indicates that the size of the dye does not affect the adsorption of the dye significantly. The RuO_2-decorated TNTs and bare TNTs seemed to degrade the methylene blue to about zero after 2 hours. The trend of the RuO_2-decorated TNTs having lower reaction rates continued from the malachite green degradation with the k_{app} for the methylene blue being 1.46×10^{-2} min^{-1} and 3.4×10^{-3} min^{-1} (bare TNTs and RuO_2-decorated TNTs respectively), while the K_{norm} reaction rates were measured to be 5.12×10^{-5} g m^{-2} min^{-1} and 1.77×10^{-5} g m^{-2} min^{-1} (bare TNTs and RuO_2-decorated TNTs respectively). The pH of the stock solution of methylene blue was 6.02 (adjusted with 0.1 M HCl). In order to obtain a better photodegradation rate, due to the high adsorbance demonstrated by the RuO_2-decorated TNTs, another methylene blue degradation Fig. 12 was conducted at a 50 ppm concentration for 240 min at pH 7.02 (not shown). The percent dye concentration of the bare TNTs began at about 0.53 and was 0.51 after 240 min., while the RuO_2-decorated TNTs began at about 0.32 and was 0.21 after 240 min. The RuO_2-decorated TNTs showed a higher photodegradation rate with a k_{app} of 1.7×10^{-3} min^{-1} and a K_{norm} of 5.84×10^{-6} g m^{-2} min^{-1}, while the bare TNTs had a k_{app} of 2×10^{-4} min^{-1} and a K_{norm} of 7.01×10^{-7} g m^{-2} min^{-1}. This photodegradation data again confirmed that the RuO_2-decorated TNTs were an improved catalyst to the bare TNTs for the methylene blue dye in terms of

adsorption. Similar to the malachite green molecules, some of the methylene blue molecules also remained on the surface of the catalyst after the UV-treatment was finished. These remaining molecules can potentially be products such as phenols and benzene rings that are toxic.[31, 46] This is visually observed by the color of the catalysts changing to black.

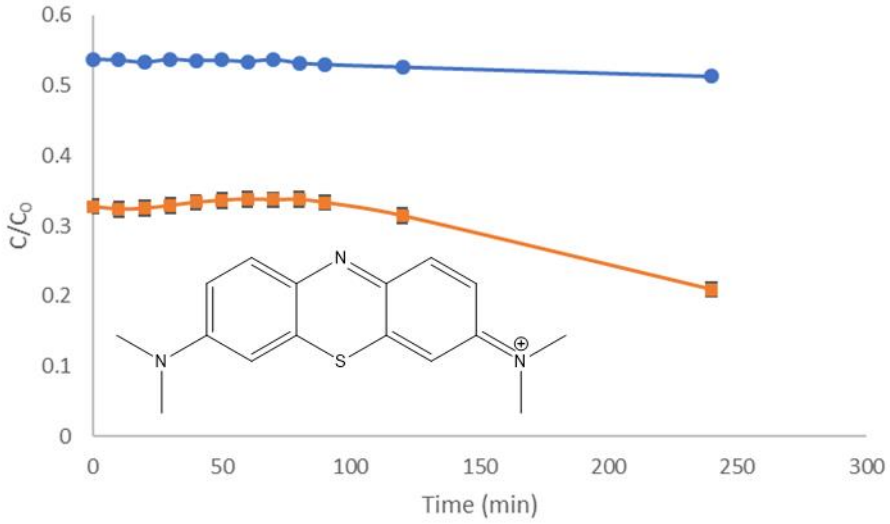

Figure 12. Plot displaying the dye concentration vs. irradiation time for the degradation of 50 ppm methylene blue (inset) with TiO_2 nanotubes (—●—) and TiO_2 nanotubes decorated with RuO_2 (—■—).

The results of Fig. 13 feature the effects of the bare TNTs and the RuO_2-decorated TNTs with an anionic dye, indigo carmine. Neither of the catalyst seemed to have any significant effect on the dye concentration while stirring in darkness, but the bare TNTs adsorbed about 10% dye concentration. This is due to the negatively-charged surface of the TiO_2-based catalysts

hindering surface adsorption by repelling the negatively charged indigo carmine, while an attractive effect was observed in the cationic dyes.[35-36] The concentration of indigo carmine only decreased during UV-irradiation, meaning no significant adsorption occurred. The dye degradation rate for the bare TNTs seems to be more efficient than the RuO_2-decorated TNTs, with the bare TNTs completing the photodegradation of the indigo carmine (pH=7.60) after 60 minutes, which was faster than the time that was required for the malachite green and methylene blue dyes. The RuO_2-decorated TNTs only degraded the indigo carmine to about 40% after 4 hours, which was slower than the time needed to remove ~95% of the cationic malachite green and methylene blue dyes. The k_{app} for the bare TNTs was 5.2×10^{-2} min^{-1} and 3.9×10^{-3} min^{-1} for the RuO_2-decorated TNTs, while the K_{norm} for the bare TNTs was 1.82×10^{-4} g m^{-2} $min^{-1}$and 1.34×10^{-5} g m^{-2} min^{-1} for the RuO_2-decorated TNTs. This slower photodegradation time for the indigo carmine maybe due to its anionic nature. The slow photodegradation rate is most likely caused by the fact that the anionic indigo carmine is not adsorbing to the surface of the catalysts like malachite green and methylene blue do. The idea of a lack of dye molecules on the surface of the catalyst is supported by the fact that no color change is observed for either catalyst after the reaction (TNTs remained white and RuO_2-decorated TNTs remained green). The surface being occupied by less dye molecules would allow the catalyst to be better stimulated by the UV-light to produce more radical species. This reaction result displayed that RuO_2 nanoparticles hinder the performance of photodegradation for anionic dyes.

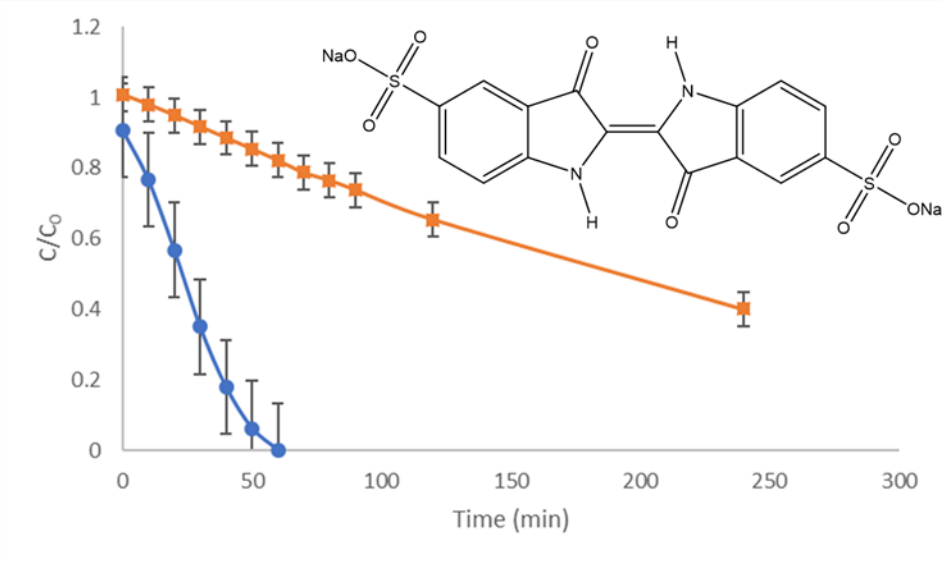

Figure 13. Plot displaying the dye concentration vs irradiation time for the degradation of indigo carmine with TiO_2 nanotubes (—●—) and TiO_2 nanotubes decorated with RuO_2(—■—).

Table 2. Dye Reaction Rate Constants

Photocatalyst	S_{BET} (m^2g^{-1})	Malachite Green k_{app} (min^{-1})	Malachite Green K_{norm} (g m^{-2} min^{-1})
TNTs	285	2.76×10^{-2}	9.67×10^{-5}
RuO_2-TNTs	290	1.16×10^{-2}	3.99×10^{-5}
		Methylene Blue k_{app} (min^{-1})	Methylene Blue K_{norm} (g m^{-2} min^{-1})
TNTs	285	1.46×10^{-2}	5.12×10^{-5}
RuO_2-TNTs	290	3.4×10^{-3}	1.77×10^{-5}
		Indigo Carmine k_{app} (min^{-1})	Indigo Carmine K_{norm} (g m^{-2} min^{-1})
TNTs	285	5.2×10^{-2}	1.82×10^{-4}
RuO_2-TNTs	290	3.9×10^{-3}	5.84×10^{-6}

3.3 Literature Comparisons

To understand the significance of our RuO_2-decorated TNT catalyst it was compared to other catalysts that have been previously reported in literature. The first catalyst our RuO_2-decorated

TNTs were compared to was RuO_2-decorated TiO_2 nanoparticles synthesized by Uddin et al.[21] Uddin et al. loaded TiO_2 nanoparticles (size ~18 nm) with 2-5 nm RuO_2 nanoparticles at loadings of 1%, 2.5%, and 5%.[21] The BET surface areas for all the loading of the RuO_2-decorated catalyst were ~70 m^2g^{-1}.[21] The photodegradation was performed on a methylene blue solution in water of 10 mg/L.[21] 0.1 g of photocatalyst was dispersed in 100 mL of dye solution at a pH of 7.[21] The 1% loaded sample preformed the best with a k_{app} of 2.39×10^{-1} min^{-1} and a K_{norm} of 3.57×10^{-3}.[21] The dye was fully degraded in 20 min.[21] The k_{app} and K_{norm} of the 1% RuO_2-decorated TiO_2 nanoparticles were superior to the k_{app} and K_{norm} for our RuO_2-decorated TNTs 3.4×10^{-3} and 1.77×10^{-5}, respectively. Two big factors for the differences in the degradation rate could be Uddin et al. uses five times more catalyst and that the pH of our solution is only 6.22, while theirs is 7. Regardless, our RuO_2-decorated TNTs show superior adsorption despite that our solution is more concentrated (25 mg/L). This superior adsorption is due to our use of the higher surface area TiO_2 nanotubes.[37] The second catalyst that was compared against our RuO_2-decorated TNTs were CuS-decorated TNTs synthesized by Ratanatawanate et al.[18] Ratanatawanate et al. loaded TNTs with 2-6 nm CuS nanoparticles.[18] The photodegradation was performed on a 0.3mM malachite green solution in water at pH 6.2.[18] 25 mg of photocatalyst was dispersed in 100 mL of the malachite green dye solution.[18] The CuS-decorated TNTs degraded the solution to ~40% in 120 min.[18] Due to the fact Ratanatawanate et al. used ~5 times as much malachite green and degraded more dye in the same time span, the CuS-decorated TNTs show better photocatalytic activity.[18] Once more the only benefit provided by the RuO_2-decorated TNTs are their adsorption capabilities. The last catalyst that was compared

to our RuO_2-decorated TNTs were PbS-decorated TNTs synthesized by Ratanatawanate et al.[20] Ratanatawanate et al. loaded TNTs with 4-5 nm PbS nanoparticles.[19] The photodegradation was performed on an indigo carmine solution in water (25 mg/L) at pH 5.7.[19] 25 mg of photocatalyst was added to the 100 mL of the dye solution and the solution was irradiated for 120 min.[19] The PbS-decorated TNTs degraded the solution to ~10%, which was better than our RuO_2-decorated TNTs that degraded the solution to ~40% in 240 min.[19] This shows that the PbS-decorated TNTs have superior photocatalytic activities, in addition the adsorption capabilities of both catalysts were negligible. Overall the main benefit of the RuO_2-decorated TNTs, when compared to similar catalyst, was their adsorption capabilities for cationic dyes.

CHAPTER 4

CONCLUSIONS

Titanium dioxide nanotubes decorated with 1-5 nm ruthenium oxide nanoparticles of sizes were synthesized. A RuO_2/TiO_2 heterojunction was indicated by the XPS results in which band bending of the conduction band occurred (indicating a Ru-O-Ti bond). Band bending was further supported by the tauc plots with 0.6 M and 0.9 M cysteine synthesized RuO_2-decorated TNTs being calculated to have lowered band gaps of 2.73 eV and 2.69 eV, respectively. The RuO_2 nanoparticles decorated TiO_2 nanotubes displayed activity for the entire spectrum of 200-1200 nm with a max near 300 nm, and a minimum near 600 nm. The cationic dyes proved to be well adsorbed before irradiation with UV-light for the RuO_2-decorated TNTs, while the adsorption of anionic dyes seemed to be adversely affected by the presence of the RuO_2 nanoparticles on the titanium oxide nanotubes. Overall RuO_2-decorated TNTs not only performed as a superior adsorbent catalyst than the bare TNTs in the cationic dyes of malachite green and methylene blue, in addition they behaved better than RuO_2-decorated TiO_2 nanoparticles.

REFERENCES

1. Diop, S., *Vital Water Graphics: An Overview of the State of the World's Fresh and Marine Waters*. UNEP/Earthprint: 2002; Vol. 1.

2. Alderman, D. J., Malachite Green: A Review. *Journal of Fish Diseases* **1985,** *8* (3), 289-298.

3. Han, F.; Kambala, V. S. R.; Srinivasan, M.; Rajarathnam, D.; Naidu, R., Tailored Titanium Dioxide Photocatalysts for the Degradation of Organic Dyes in Wastewater Treatment: A Review. *Applied Catalysis A: General* **2009,** *359* (1-2), 25-40.

4. Berberidou, C.; Kitsiou, V.; Lambropoulou, D. A.; Antoniadis, A.; Ntonou, E.; Zalidis, G. C.; Poulios, I., Evaluation of An Alternative Method for Wastewater Treatment Containing Pesticides using Solar Photocatalytic Oxidation and Constructed Wetlands. *J Environ Manage* **2017,** *195* (Pt 2), 133-139.

5. Sacco, O.; Vaiano, V.; Rizzo, L.; Sannino, D., Photocatalytic Activity of a Visible Light Active Structured Photocatalyst Developed for Municipal Wastewater Treatment. *Journal of Cleaner Production* **2018,** *175*, 38-49.

6. Dong, H.; Zeng, G.; Tang, L.; Fan, C.; Zhang, C.; He, X.; He, Y., An Overview on Limitations of TiO2-Based Particles for Photocatalytic Degradation of Organic Pollutants and the Corresponding Countermeasures. *Water Res* **2015,** *79*, 128-46.

7. Fujishima, A.; Honda, K., Electrochemical Photolysis of Water at a Semiconductor Electrode. *Nature* **1972,** *238* (5358), 37-38.

8. Linsebigler, A. L.; Lu, G.; Yates, J. T., Photocatalysis on TiO_2 Surfaces: Principles, Mechanisms, and Selected Results. *Chemical Reviews* **1995,** *95* (3), 735-758.

9. Konaka, R.; Kasahara, E.; Dunlap, W. C.; Yamamoto, Y.; Chien, K. C.; Inoue, M., Irradiation of Titanium Dioxide Generates Both Singlet Oxygen and Superoxide Anion. *Free Radic. Biol. Med.* **1999,** *27* (3-4), 294-300.

10. Murakami, Y.; Kenji, E.; Nosaka, A. Y.; Nosaka, Y., Direct Detection of OH Radicals Diffused to the Gas Phase from the UV-Irradiated Photocatalytic TiO_2 Surfaces by Means of Laser-Induced Fluorescence Spectroscopy. *J Phys Chem B* **2006,** *110* (34), 16808-11.

11. Sekino, T., Synthesis and Applications of Titanium Oxide Nanotubes. *Topics in Applied Physics Inorganic and Metallic Nanotubular Materials* **2010,** *117*, 17-32.

12. Chen, X.; Mao, S. S., Titanium Dioxide Nanomaterials: Synthesis, Properties, Modifications, and Applications. *Chem Rev* **2007,** *107* (7), 2891-959.

13. Liu, N.; Chen, X.; Zhang, J.; Schwank, J. W., A Review on TiO_2-Based Nanotubes Synthesized via Hydrothermal Method: Formation Mechanism, Structure Modification, and Photocatalytic Applications. *Catalysis Today* **2014,** *225*, 34-51.

14. Roy, P.; Berger, S.; Schmuki, P., TiO_2 nanotubes: Synthesis and Applications. *Angew Chem Int Ed Engl* **2011,** *50* (13), 2904-39.

15. Sadegh, H.; Ali, G. A. M.; Gupta, V. K.; Makhlouf, A. S. H.; Shahryari-ghoshekandi, R.; Nadagouda, M. N.; Sillanpää, M.; Megiel, E., The Role of Nanomaterials as Effective Adsorbents and Their Applications in Wastewater Treatment. *Journal of Nanostructure in Chemistry* **2017,** *7* (1), 1-14.

16. Nakata, K.; Fujishima, A., TiO_2 Photocatalysis: Design and Applications. *Journal of Photochemistry and Photobiology C: Photochemistry Reviews* **2012,** *13* (3), 169-189.

17. Nian, J. N.; Teng, H. S., Hydrothermal Synthesis of Single-Crystalline Anatase TiO_2 Nanorods with Nanotubes as the Precursor. *J Phys Chem B* **2006,** *110* (9), 4193-4198.

18. Ratanatawanate, C.; Bui, A.; Vu, K.; Balkus, K. J., Low-Temperature Synthesis of Copper(II) Sulfide Quantum Dot Decorated TiO_2 Nanotubes and Their Photocatalytic Properties. *The Journal of Physical Chemistry C* **2011,** *115* (14), 6175-6180.

19. Ratanatawanate, C.; Tao, Y.; Balkus, K. J., Photocatalytic Activity of PbS Quantum Dot/TiO2 Nanotube Composites. *J Phys Chem C* **2009,** *113* (24), 10755-10760.

20. Ratanatawanate, C.; Xiong, C.; Balkus, K. J., Fabrication of PbS Quantum Dot Doped TiO_2 Nanotubes. *ACS Nano* **2008,** *2* (8), 1682-1688.

21. Uddin, M. T.; Nicolas, Y.; Olivier, C.; Toupance, T.; Müller, M. M.; Kleebe, H.-J.; Rachut, K.; Ziegler, J.; Klein, A.; Jaegermann, W., Preparation of RuO_2/TiO_2 Mesoporous Heterostructures and Rationalization of Their Enhanced Photocatalytic Properties by Band Alignment Investigations. *The Journal of Physical Chemistry C* **2013,** *117* (42), 22098-22110.

22. Belhadj, H.; Hamid, S.; Robertson, P. K. J.; Bahnemann, D. W., Mechanisms of Simultaneous Hydrogen Production and Formaldehyde Oxidation in H_2O and D_2O Over Platinized TiO_2. *ACS Catalysis* **2017,** *7* (7), 4753-4758.

23. Du, P.; Chang, J.; Zhao, H.; Liu, W.; Dang, C.; Tong, M.; Ni, J.; Zhang, B., Sea-Buckthorn-Like MnO_2 Decorated Titanate Nanotubes with Oxidation Property and Photocatalytic Activity for Enhanced Degradation of 17β-Estradiol under Solar Light. *ACS Applied Energy Materials* **2018,** *1* (5), 2123-2133.

24. Bavykin, D.; Lapkin, A.; Plucinski, P.; Friedrich, J.; Walsh, F., TiO_2 Nanotube-Supported Ruthenium(III) Hydrated Oxide: A Highly Active Catalyst for Selective Oxidation of Alcohols by Oxygen. *Journal of Catalysis* **2005,** *235* (1), 10-17.

25. Lačnjevac, U. Č.; Radmilović, V. V.; Radmilović, V. R.; Krstajić, N. V., RuOx Nanoparticles Deposited on TiO_2 Nanotube Arrays by Ion-Exchange Method as Electrocatalysts for the Hydrogen Evolution Reaction in Acid Solution. *Electrochimica Acta* **2015,** *168*, 178-190.

26. Tilley, S. D.; Schreier, M.; Azevedo, J.; Stefik, M.; Graetzel, M., Ruthenium Oxide Hydrogen Evolution Catalysis on Composite Cuprous Oxide Water-Splitting Photocathodes. *Advanced Functional Materials* **2014,** *24* (3), 303-311.

27. Trasatti, S., Electrocatalysis: Understanding the Success of DSA®. *Electrochimica Acta* **2000,** *45* (15-16), 2377-2385.

28. Patake, V. D.; Lokhande, C. D., Chemical Synthesis of Nano-Porous Ruthenium Oxide (RuO_2) Thin Films for Supercapacitor Application. *Applied Surface Science* **2008,** *254* (9), 2820-2824.

29. Chen, C. C.; Lu, C. S.; Chung, Y. C.; Jan, J. L., UV Light Induced Photodegradation of Malachite Green on TiO_2 Nanoparticles. *J Hazard Mater* **2007,** *141* (3), 520-528.

30. Taniguchi, M.; Lindsey, J. S., Database of Absorption and Fluorescence Spectra of >300 Common Compounds for use in PhotochemCAD. *Photochem Photobiol* **2018,** *94* (2), 290-327.

31. Houas, A., Photocatalytic Degradation Pathway of Methylene Blue in Water. *Applied Catalysis B: Environmental* **2001,** *31* (2), 145-157.

32. Kang, X.; Chen, S., Photocatalytic Reduction of Methylene Blue by TiO_2 Nanotube Arrays: Effects of TiO_2 Crystalline Phase. *Journal of Materials Science* **2010,** *45* (10), 2696-2702.

33. Lachheb, H.; Puzenat, E.; Houas, A.; Ksibi, M.; Elaloui, E.; Guillard, C.; Herrmann, J.-M., Photocatalytic Degradation of Various Types of Dyes (Alizarin S, Crocein Orange G, Methyl Red, Congo Red, Methylene Blue) in Water by UV-Irradiated Titania. *Applied Catalysis B: Environmental* **2002,** *39* (1), 75-90.

34. Natarajan, T. S.; Bajaj, H. C.; Tayade, R. J., Preferential Adsorption Behavior of Methylene Blue Dye onto Surface Hydroxyl Group Enriched TiO_2 Nanotube and its Photocatalytic Regeneration. *J Colloid Interface Sci* **2014,** *433*, 104-114.

35. Sandoval, A.; Hernández-Ventura, C.; Klimova, T. E., Titanate Nanotubes for Removal of Methylene Blue Dye by Combined Adsorption and Photocatalysis. *Fuel* **2017,** *198*, 22-30.

36. Xiong, L.; Sun, W.; Yang, Y.; Chen, C.; Ni, J., Heterogeneous Photocatalysis of Methylene Blue Over Titanate Nanotubes: Effect of Adsorption. *J Colloid Interface Sci* **2011,** *356* (1), 211-6.

37. Xiong, L.; Yang, Y.; Mai, J.; Sun, W.; Zhang, C.; Wei, D.; Chen, Q.; Ni, J., Adsorption Behavior of Methylene Blue onto Titanate Nanotubes. *Chemical Engineering Journal* **2010,** *156* (2), 313-320.

38. Zanoni, T. B.; Cardoso, A. A.; Zanoni, M. V. B.; Ferreira, A. A. P., Exploratory Study on Sequestration of Some Essential Metals by Indigo Carmine Food Dye. *Brazilian Journal of Pharmaceutical Sciences* **2010,** *46* (4), 723-730.

39. Morrison, G.; Fatoki, O. S.; Persson, L.; Ekberg, A., Assessment of the Impact of Point Source Pollution from the Keiskammahoek Sewage Treatment Plant on the Keiskamma River - pH, Electrical Conductivity, Oxygen- Demanding Substance (COD) and Nutrients. *Water SA* **2001,** *27* (4), 475-480.

40. Akpan, U. G.; Hameed, B. H., Parameters Affecting the Photocatalytic Degradation of Dyes Using TiO_2-Based Photocatalysts: A Review. *J Hazard Mater* **2009,** *170* (2-3), 520-9.

41. Luxton, T. P.; Eick, M. J.; Scheckel, K. G., Characterization and Dissolution Properties of Ruthenium Oxides. *J Colloid Interface Sci* **2011,** *359* (1), 30-39.

42. Erdem, B.; Hunsicker, R. A.; Simmons, G. W.; Sudol, E. D.; Dimonie, V. L.; El-Aasser, M. S., XPS and FTIR Surface Characterization of TiO_2 Particles Used in Polymer Encapsulation. *Langmuir* **2001,** *17* (9), 2664-2669.

43. Rochefort, D.; Dabo, P.; Guay, D.; Sherwood, P. M. A., XPS Investigations of Thermally Prepared RuO_2 Electrodes in Reductive Conditions. *Electrochimica Acta* **2003,** *48* (28), 4245-4252.

44. Jürgensen, A.; Raschke, H.; Esser, N.; Hergenröder, R., An In situ XPS Study of L-cysteine Co-Adsorbed with Water on Polycrystalline Copper and Gold. *Applied Surface Science* **2018,** *435*, 870-879.

45. Ganguly, B. N.; Maity, B.; Maity, T. K.; Manna, J.; Roy, M.; Mukherjee, M.; Debnath, S.; Saha, P.; Shilpa, N.; Rana, R. K., L-Cysteine-Conjugated Ruthenium Hydrous Oxide Nanomaterials with Anticancer Active Application. *Langmuir* **2018,** *34* (4), 1447-1456.

46. Prado, A. G.; Costa, L. L., Photocatalytic Decouloration of Malachite Green Dye by Application of TiO_2 Nanotubes. *J Hazard Mater* **2009,** *169* (1-3), 297-301.

BIOGRAPHICAL SKETCH

Jonathan Daniel Buford was born in Seattle, Washington in 1993. He moved to Richardson, Texas in 1999. He obtained his Bachelor of Science in Chemistry with a minor in mathematics from Texas Tech University in 2015. In fall 2015, he entered The University of Texas at Dallas to pursue his graduate studies under the instruction of Dr. Kenneth J. Balkus, Jr. His research focused on metal oxide materials and their applications.

CURRICULUM VITAE

Jonathan D. Buford

Address:

Email: jxb110930@utdallas.edu

Education

B.S. Chemistry, 2015, Texas Tech University

M.S. Chemistry 2018, University of Texas at Dallas

Professional Experience

Formed titanium oxide nanotube decorated with ruthenium oxide nanoparticles via hydrothermal synthesis for the photocatalytic purification of water.

Studied Energy Storage for supercapacitors with a focus on metal oxide materials, metal oxide carbon hybrid materials, and metal organic framework materials.

Research Interests

Catalysis

Energy Storage

Metal oxide materials

Publications

N/A

Conference Presentations

J. D. Buford, K. J. Balkus Jr.; "TiO_2 Nanotubes Decorated with Ruthenium-based Nanoparticles" 51st Annual DFW ACS Meeting in Miniature, Texas Christian University (April 2017, Fort Worth TX)

J. D. Buford, K. J. Balkus Jr.; "TiO_2 Nanotubes Decorated with Ruthenium-based Nanoparticles" 51^{st} Annual DFW ACS Meeting in Miniature, Southern Methodist University (April 2018, Dallas TX)

Technical Skills

Materials Chemist

X-ray diffraction (XRD), Scanning electron microscopy (SEM), Transmission electron microscopy (TEM), Infrared spectroscopy (FTIR and ATR), Ultraviolet-visible spectroscopy (UV-Vis: including solid state)

Awards & Honors

N/A

Languages

English

Professional Memberships

Member of the American Chemical Society 2012-present